Journal of Sciences, Islamic Republic of Iran 25(2): 175 - 183 (2014) http://jsciences.ut.ac.ir
University of Tehran, ISSN 1016-1104

Effective Mechanical Properties of Nanocomposites Reinforced With Carbon Nanotubes Bundle

M. Hashemi Gahruei[1], and H. Golestanian[*1, 2]

[1] *Department of Mechanical Engineering, Faculty of Engineering,University of Shahrekord, Shahrekord, 8818634141, Islamic Republic of Iran*
[2] *Nanotechnology Research Center, University of Shahrekord, Shahrekord, 8818634141, Islamic Republic of Iran*

Received: 26 January 2014 / Revised: 28 June 2014 / Accepted: 5 July 2014

Abstract

Nanocomposites made of Carbon Nanotube (CNT) bundles have attracted researchers' attention due to their unusual properties such as: light weight, flexibility and stiffness. In this paper, the effects of straight and rope-shaped bundles on nanocomposite effective mechanical properties are investigated. First, FEA models are created consisting of CNTs with different shapes of straight and rope-shaped bundles to investigate the effects of straight and rope-shaped bundles dimensions. Next, the reinforcing efficiency of CNTs in different matrices is investigated using models consisting of matrices with different moduli of elasticity. The results show that the increases of Young's modulus of matrix and straight bundle and rope-shaped bundle diameter can significantly reduce the stiffening effect of the nanotubes in longitudinal fiber and increase the stiffening effect of the nanotubes in transverse fiber. Also, Young's modulus prediction for carbon nanotube in a poly (ethylene terephthalate) matrix is compared to experimental data investigated by Gómez-del Río et al. (2010), and good agreement is observed.

Keywords: Carbon Nanotube; Straight Bundle; Rope-shaped Bundle; Nanocomposite; Effective Mechanical Properties.

Introduction

Since the discovery of carbon nanotubes (CNTs) by Iijima [1], interest in CNTs has grown very rapidly because of their unique and superior properties. Both experimental and theoretical studies have shown that CNTs have extraordinary mechanical and electrical properties [2, 3]. For example, numerous theoretical and experimental results have shown that both single-walled carbon nanotubes (SWCNTs) and multi-walled carbon nanotubes (MWCNTs) have Young's modulus about 1 TPa in the axial direction, depending on the diameter and chirality [4, 5]. CNTs are often free of defects, leading to their very high tensile strength. By measuring the mechanical response of CNTs under tension, Yu et al. [6, 7] obtained the tensile strength of SWCNTs ranging from 13 to 52 GPa, and reported the tensile strength of individual MWCNTs in the range from 11 to 63 GPa.

Because of their unique structural, mechanical and electronic properties [1–7], carbon nanotubes have been considered for numerous potential applications, such as super strong fibers [8], nanoelectronic devices [9, 10],

[*] Corresponding author: Tel: +983814424438; Fax: +98213814424438; Email: golestanian@eng.sku.ac.ir

and nanocomposites [11]. However for some applications, especially in mechanical applications, it is hampered by the difficulty experienced in producing specified nanotube-based macroscopic structures. The synthesis of these materials has become one of the highlights in recent nanocomposite research [12].

Golestanian and Shojaie investigated the influence of CNT/matrix interface properties on nanocomposite mechanical properties. They found that by increasing the interface strength between the nanotube and the matrix, strengthening efficiency of nanotube increases. They considered perfect bonding and elastic interface cases in their simulations [13]. Mechanical properties of a single nanotube [14, 15], the functionalization and purification of CNTs [16, 17], and the constitutive modeling of a single nanotube including the local polymer surrounding the nanotube and the nanotube/polymer interface [18, 19] have been extensively studied. However, it is recognized that there is still much needed research before we can manufacture CNT reinforced composites that fully realize the potentials of high stiffness and strength of CNTs. Many parameters influence mechanical properties of nanocomposites such as: CNT configuration, dispersion, alignment, and volume fraction as well as matrix properties. Most experimental investigations of carbon nanotube/ polymer composites [20–22] involve carbon nanotube bundles or ropes instead of individual tubes because CNTs often form bundles or ropes in real nanocomposites due to Van der Waals interactions between tubes.

Bundles of carbon nanotube and rope-shaped carbon nanotubes are attracting great interest for their unusual properties [23, 24]. Single-walled nanotubes are usually assembled into macroscopic bundles by Van der Waals interactions [25, 26], whereas multi-walled carbon nanotubes (MWNTs) generally come either as disordered individual tubes or aligned CNTs array [27]. Klaus [28] reported the presence of bundles of MWNT. Ning et al. [29] produced MWNT bundles on sol-gel prepared catalyst. Zhang et al. [30] also produced MWNT bundles by first depositing a film of amorphous carbon on quartz substrate.

In this paper, an effort is made to model straight and rope-shaped bundles CNT-based nanocomposites at the continuum level based on the multi-scale homogenization theory and finite element method. Relations based on the elasticity theory for extracting the effective material properties from solutions of the square RVE are derived. Then, numerical models are created to determine nanocomposite effective mechanical properties. Finite element models are created to investigate the effects of rope shape and matrix modulus on nanocomposite effective mechanical properties.

Materials and Methods

Analysis

To simplify the analysis, we will treat the nanotubes as solid short fibers. Parameters of straight bundle of CNT's (SBCNT's) and rope-shaped bundle of CNT's (RBCNT's) are shown in Fig. (1) a and b. In these figures D is the rope-shaped bundle or straight bundle diameter, d is the diameter of CNTs in the assembly, and L is the rope-shaped bundle or straight bundle length. Also, perfect bonding is assumed at the rope-shaped bundle /matrix or straight bundle /matrix

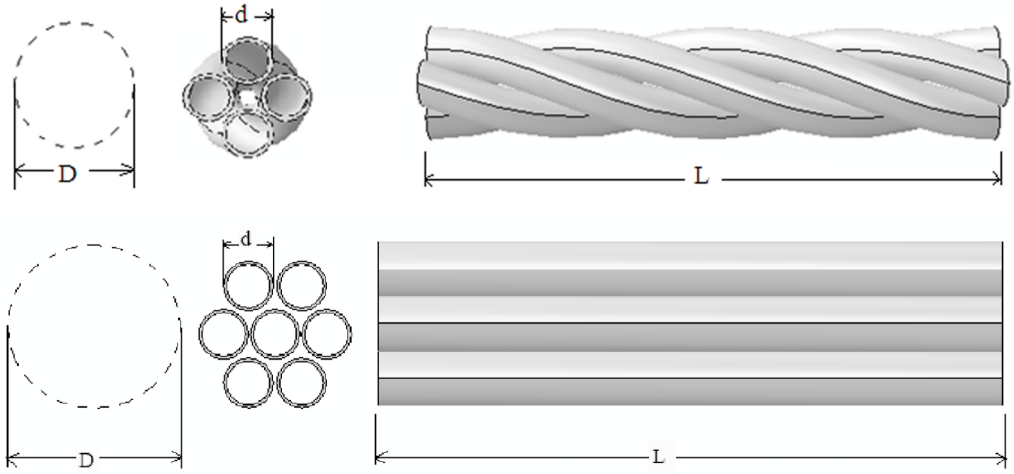

Figure 1. Configuration of (a) rope-shaped bundle of CNT's and (b) straight bundle of CNT's

interface. The analysis approach and the formulations are presented in the next sections.

Extracting the Effective Material Constants

In this investigation, the analysis is performed on a square RVE consisting of a straight fiber inside the matrix. A cut-through view of the RVE is shown in Fig. 2. To derive the relations for extracting the effective nanocomposite mechanical properties, a homogenized elasticity model of the square RVE is modeled. The geometry of the elasticity model corresponds to a solid square RVE with length L and cross-sectional area 2a × 2a (Fig. 3-a).

Elasticity solutions can be obtained under certain load cases. The elasticity model is filled with a single, transversely isotropic material that has five independent material constants. The four effective material constants (Young's moduli E_x and E_z, and Poisson s ratios ν_{xy} and ν_{zx}, relating the normal stress and strain components) will be determined. See Fig. 2 for the orientation of the coordinates. The fifth independent material constant, the shear modulus G_{xz} (= G_{yz}), can be obtained using a simple torsional load case and will not be considered in this paper. The general 3-D strain–stress relation relating the normal stresses and strains for a transversely isotropic material can be written as [31, 32]:

$$\begin{Bmatrix} \varepsilon_x \\ \varepsilon_y \\ \varepsilon_z \end{Bmatrix} = \begin{bmatrix} \frac{1}{E_x} & -\frac{\nu_{xy}}{E_x} & -\frac{\nu_{zx}}{E_z} \\ -\frac{\nu_{xy}}{E_x} & \frac{1}{E_x} & -\frac{\nu_{zx}}{E_z} \\ -\frac{\nu_{zx}}{E_z} & -\frac{\nu_{zx}}{E_z} & \frac{1}{E_z} \end{bmatrix} \begin{Bmatrix} \sigma_x \\ \sigma_y \\ \sigma_z \end{Bmatrix} \quad (1)$$

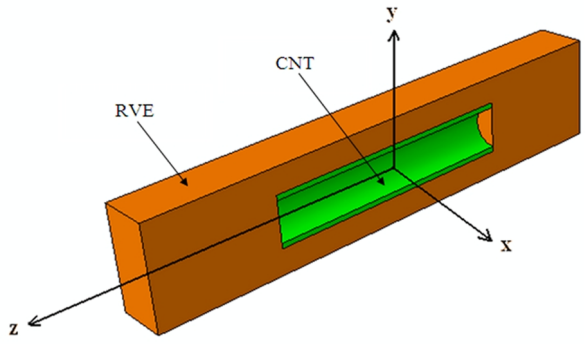

Figure 2. A square RVE containing a short CNT shown in a cut through view.

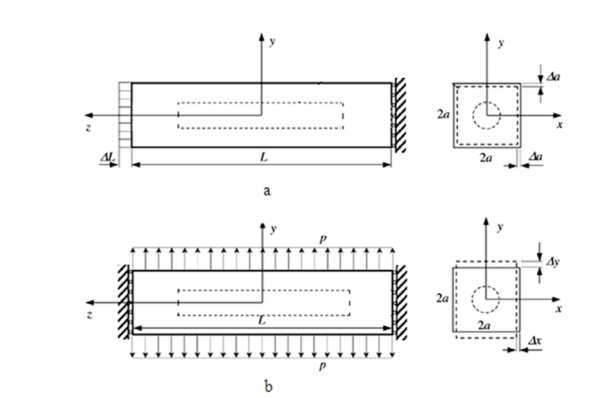

Figure 3. Two loading cases applied to the square RVE. (a) an axial elongation ΔL in the z- direction; (b) lateral distributed load, p, in the y- direction

To determine the four unknown material constants (E_x, E_z, ν_{xy} and ν_{zx}), four equations will be needed. Two loading cases have been devised to provide four such equations based on the elasticity theory. These loading cases are illustrated in Fig. 3 and will be discussed in the next sections.

Square RVE under an axial elongation ΔL

In this load case (Fig. 3(a)), the RVE is loaded by an arbitrary elongation in the z direction. The stress and strain components on the lateral surface are:

$$\sigma_x = \sigma_y = 0, \text{ and } \sigma_z = \sigma_{ave}$$
$$\varepsilon_x = \frac{\Delta a}{a}, \qquad \varepsilon_z = \frac{\Delta L}{L}, \text{ along x=±a}$$
And; (2)
$$\varepsilon_y = \frac{\Delta a}{a}, \quad \text{along y=±a}$$

Where Δa is the change of dimension a of the RVE cross-section under the elongation ΔL. Integrating and averaging the third equation in (1) on the plane z=L/2, we have;

$$E_z = \frac{\sigma_z}{\varepsilon_z} = \frac{L}{\Delta L}\sigma_{ave} \quad (3)$$

Where the averaged value of stress σ_{ave} is given by:

$$\sigma_{ave} = \frac{1}{A}\int \sigma_x(x, y, L/2)dxdy \quad (4)$$

With A being the RVE cross sectional area. The value of σ_{ave} is evaluated for the RVE using the FEM results as follows:

$$\sigma_{ave} = \frac{\sigma_{CNT} A_{CNT} + \sigma_{matrix} A_{matrix}}{A} \quad (5)$$

Using the first relation in Eq. (1) along with Eq. (2), we can write;

$$\varepsilon_x = -\frac{\nu_{zx}}{E_z}\sigma_{ave}$$

$$\nu_{zx} = -\frac{\varepsilon_x}{\sigma_{ave}} E_z = -\frac{\frac{\Delta a}{a}}{\frac{\Delta L}{L}} \quad (6)$$

Along x=±a

Once the contraction Δa and the stress σ_{ave} in case (a) are obtained from FEA models, Eqs. (3) and (6) can be solved to determine the effective Young's modulus E_z and Poisson's ratio ν_{zx} (=ν_{zy}).

Square RVE under a lateral distributed load p (Fig. 3-b)

In this load case (Fig. 3(b)), the square RVE is loaded with a uniformly distributed load (negative pressure), p, in the y-direction. The RVE is constrained in the z -direction so that the plane strain condition is maintained, in order to simulate the interactions of the RVE with surrounding matrix material in the z-direction.

Due to the plane strain conditions, we have:

$$\varepsilon_z = 0, \quad \sigma_z = \nu_{zx}(\sigma_x + \sigma_y) \quad (7)$$

In this case, the 3-D stress–strain relation (1) reduces to:

$$\begin{Bmatrix} \varepsilon_x \\ \varepsilon_y \end{Bmatrix} = \begin{bmatrix} \frac{1}{E_x} - \frac{\nu_{zx}^2}{E_z} & \frac{\nu_{xy}}{E_x} - \frac{\nu_{zx}^2}{E_z} \\ \frac{\nu_{xy}}{E_x} - \frac{\nu_{zx}^2}{E_z} & \frac{1}{E_x} - \frac{\nu_{zx}^2}{E_z} \end{bmatrix} \begin{Bmatrix} \sigma_x \\ \sigma_y \end{Bmatrix} \quad (8)$$

For the corresponding elasticity model (Fig. 3(b)), one has the following results for the normal stress and strain components at a point on the lateral surfaces:

$$\varepsilon_x = \frac{\Delta x}{a}, \text{ along x=±a}, \quad \sigma_x = 0, \quad \sigma_y = P$$

$$\varepsilon_y = \frac{\Delta y}{a}, \qquad \text{along y=±a} \quad (9)$$

Where Δx and Δy are the changes of dimensions in the x-and y-directions, respectively. Applying the first equation in (8) for points along x = ±a and the second equation in (4) for points along y =±a, we obtain:

$$\varepsilon_x = -(\frac{\nu_{xy}}{E_x} + \frac{\nu_{zx}^2}{E_z})P = \frac{\Delta x}{a}$$

$$\varepsilon_y = (\frac{1}{E_x} - \frac{\nu_{zx}^2}{E_z})P = \frac{\Delta y}{a} \quad (10)$$

By solving these two equations, we can determine the effective Young's modulus and Poisson's ratio in the transverse direction (xy plane, Fig. 2):

$$E_x = E_y = \frac{1}{\frac{\Delta y}{Pa} + \frac{\nu_{zx}^2}{E_z}} \quad (11)$$

$$\nu_{xy} = -\frac{\frac{\Delta x}{Pa} + \frac{\nu_{zx}^2}{E_z}}{\frac{\Delta y}{Pa} + \frac{\nu_{zx}^2}{E_z}} \quad (12)$$

Numerical Modeling

Several FEA models consisting of a single straight, a straight bundle and a roped-shaped bundle of CNT's in a matrix material were created using ABAQUS finite element software in order to determine the effective mechanical properties of the CNT-based nanocomposite. The dimensions of the RVE, and the constituents in these models are listed in Tables 1 through 3. The values of the dimensions and material constants are within the wide ranges reported for CNTs [33-37]. Based on these RVE and CNT dimensions fiber volume fraction in the RVE for all three models is 1.4 percent. Material properties of the constituents are listed in Table 4. Matrix modulus is varied from 2.6 to 100 GPa to investigate the effects of matrix strength on nanocomposite mechanical properties.

First, the deformations and stresses were determined for all two loading cases (Fig. 4) as described in Section 3. The FEM results were then processed and Eqs. (3), (6), (11) and (12) were used to determine the effective Young's moduli and Poisson's ratios of the nanocomposites. In all three cases, tetrahedral elements were used to mesh the 3-D models. The results of this investigation are presented in the following sections for each case.

Table 1. Dimensions of the RVE and single of straight CNT (SSCNT) used in the models.

RVE	SSCNT
Length = 100 nm 2a = 20	Length = 50 nm d=10 nm Thickness = 0.34 nm

Table 2. Dimensions of the SBCNT's models 1 and 2.

SBCNT's- model (1)		SBCNT's-model (2)	
Length = 50 nm	D=30	Length = 50 nm	D=10
Thickness = 0.34 nm	d=10	Thickness = 0.34 nm	d=3.3

Table 3. Dimensions of the RBCNT's in models 1 and 2.

RBCNT's- model (1)		RB CNT's- model (2)	
Length = 50 nm	D=25	Length = 50 nm	D=10
Thickness = 0.34 nm	d=10	Thickness = 0.34 nm	d=4

Table 4. Mechanical properties of the constituent used in the models.

Constituent	Young's Modulus (GPa)	Poisson's Ratio
Matrix	2.6 to 100	0.3
CNT	1000	0.3

Results and Discussion

First, the proposed method is validated by comparing the predicted axial modulus with those found in the literature. In Fig. 4 Young's modulus prediction for carbon nanotube in a poly (ethylene terephthalate) matrix (E = 2.6 GPa, ν = 0.438) is compared to experimental data [37].

As can be seen in Fig. 4, the results of the current investigation are in good agreement with the experimental values.

After verification of our approach, models were created to investigate the effects of matrix Young's modulus and straight and rope-shaped bundles dimensions on nanocomposite mechanical properties.

Next, models were created to investigate the effects of matrix Young's modulus on nanocomposite mechanical properties. The results of this investigation are listed in Table 5. These results correspond to the nanocomposite with a SSCNT with volume fraction of 1.40%, and $(L/d)_{SSCNT's} = 5$' Nanocomposite transverse modulus and Poisson's ratios are also listed in Table 5. As can be seen in Table 5, the ratio of nanocomposite longitudinal modulus to matrix modulus decreases as matrix modulus increases from 2.6 to 100 GPa. Note that the strengthening effect of the CNT decreases as the matrix modulus increases. These results indicate a higher efficiency of the nanotube in raising nanocomposite effective modulus when the difference between constituent moduli is large. The transverse modulus of the nanocomposite, however, turned out to be lower than the matrix modulus and increased with matrix modulus. These results suggest that the CNT acts as a cavity and actually weakens the matrix in the transverse directions.

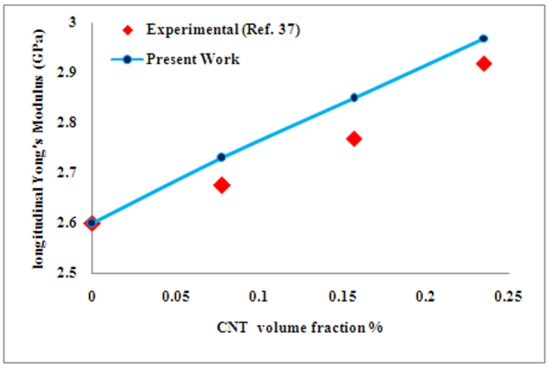

Figure 4. Comparison between Present work and experiment on elastic properties of CNT/poly (ethylene terephthalate) nanocomposite [37]

Next, the nanocomposite consisting of the SBCNT's was created in which the CNT diameter is equal to a

Table 5. Numerical results for various matrix moduli. (CNT volume fraction 1.40 %, $(L/d)_{SSCNT's} = 5$)

E_m (GPa)	E_z/E_m	E_x/E_m	ν_{zx}	ν_{xy}
2.6	1.487	0.9335	0.4336	0.2575
3.2	1.472	0.9373	0.4287	0.2586
5	1.432	0.9436	0.4155	0.2632
10	1.355	0.9546	0.3957	0.2714
15	1.304	0.9643	0.3810	0.2763
20	1.262	0.9707	0.3704	0.2795
50	1.103	0.9904	0.3301	0.2871
70	1.065	0.9952	0.3157	0.2884
100	1.026	0.9996	0.3030	0.2907

Table 6. Numerical results for various matrix moduli. (SBCNT's-model-1) (CNT volume fraction 1.40%, L/d=5, $(L/d)_{SBCNT's}$=1.67)

E_m (GPa)	E_z/E_m	E_x/E_m	ν_{zx}	ν_{xy}
2.6	1.3852	0.9433	0.4206	0.2635
3.2	1.3765	0.9476	0.4187	0.2646
5	1.3479	0.9510	0.4105	0.2682
10	1.2925	0.9633	0.3853	0.2764
15	1.2490	0.9723	0.3710	0.2812
20	1.2149	0.9805	0.3601	0.2845
50	1.0809	1.0081	0.3211	0.2921
70	1.0447	1.0182	0.3067	0.2934
100	1.0099	1.0277	0.2965	0.2937

Table 7. Numerical results for various matrix moduli. (SBCNT's-model-2) (CNT volume fraction 1.40%, L/d=15, $(L/d)_{SBCNT's}$=5)

E_m (GPa)	E_z/E_m	E_x/E_m	ν_{zx}	ν_{xy}
2.6	1.5536	0.9285	0.4441	0.2523
3.2	1.5395	0.9323	0.4410	0.2539
5	1.4935	0.9356	0.4327	0.2581
10	1.4195	0.9466	0.4139	0.2655
15	1.3655	0.9563	0.3996	0.2699
20	1.3234	0.9627	0.3883	0.2735
50	1.1808	0.9837	0.3507	0.2840
70	1.1401	0.9880	0.3382	0.2865
100	1.0985	0.9918	0.3268	0.2892

SSCNT. This case will be called model 1 from here on. Models were created to investigate the effects of CNT configuration and matrix Young's modulus on nanocomposite mechanical properties. The ratios of the nanocomposite longitudinal and transverse moduli to matrix modulus are listed in Table 6. These results correspond to the nanocomposite with a SBCNT's and volume fraction of 1.40%, L/d = 5, $(L/d)_{SBCNT's}$ = 1.67. Nanocomposite transverse modulus and Poisson's ratios are also listed in Table 6. Note that the longitudinal modulus of the nanocomposite reinforced with SBCNT's is lower than that of the SSCNT. The reason is the small aspect ratio of SBCNT's compared to the SSCNT. However, note that the transverse modulus, E_x, for nanocomposite reinforced with SBCNT's is higher than that of nanocomposite reinforced with SSCNT. The reason is the small aspect ratio of SBCNT's compared to the SSCNT and invigorate of SBCNT's in the transverse direction.

Then SBCNT's (model-2) is created which diameter of SBCNT's is equal to SSCNT. Models were created to investigate the effects of matrix Young's modulus, on nanocomposite mechanical properties. The ratios of the nanocomposite longitudinal and transverse moduli to matrix modulus are listed in Table 7. These results correspond to the nanocomposite with a SBCNT's and volume fraction of 1.40%, and L/d = 15, $(L/d)_{SBCNT's}$=5. Nanocomposite transverse modulus and Poisson's ratios are also listed in this table. Comparison results obtained with result of nanocomposite reinforced with SSCNT is shown which of E_z for nanocomposite reinforced with SBCNT's is larger E_z for nanocomposite reinforced with SSCNT. The reason is large aspect ratio of CNT's of straight bundle than single straight CNT's. But in transverse direction, E_x for nanocomposite reinforced with SBCNT's is smaller E_x for nanocomposite reinforced with single of CNT. The reason is large aspect ratio of CNT's of straight bundle than single of CNT's and single of CNT with same diameter with SBCNT's has greater Solidarity in the transverse direction than SBCNT's.

Then RBCNT's (molel-1) is created which diameter of CNT's of rope is equal to SSCNT. Models were created to investigate the effects of matrix Young's modulus, on nanocomposite mechanical properties. The ratios of the nanocomposite longitudinal and transverse moduli to matrix modulus are listed in Table 8. These results correspond to the nanocomposite with a RBCNT's and volume fraction of 1.40%, and L/d = 5, $(L/d)_{RBCNT's}$=2. Nanocomposite transverse modulus

Table 8. Numerical results for various matrix moduli. (RBCNT's-model-1) (CNT volume fraction 1.40%, L/d=5, $(L/d)_{RBCNT's}$=2)

E_m (GPa)	E_z/E_m	E_x/E_m	ν_{zx}	ν_{xy}
2.6	1.2776	0.9403	0.4113	0.2675
3.2	1.2638	0.9431	0.4054	0.2686
5	1.2285	0.9489	0.3972	0.2712
10	1.1676	0.9601	0.3713	0.2794
15	1.1275	0.9689	0.3549	0.2842
20	1.0985	0.9755	0.3425	0.2875
50	1.0107	0.9969	0.3058	0.2951
70	0.9829	1.0068	0.2942	0.2964
100	0.9568	1.0153	0.2834	0.2968

Table 9. Numerical results for various matrix moduli. (RBCNT's-model-2) (CNT volume fraction 1.40%, L/d=12.5, $(L/d)_{RBCNT's}$=5)

E_m (GPa)	E_z/E_m	E_x/E_m	ν_{zx}	ν_{xy}
2.6	1.5256	0.9295	0.4424	0.2480
3.2	1.5124	0.9353	0.4399	0.2482
5	1.4878	0.9396	0.4276	0.2531
10	1.3959	0.9506	0.4059	0.2607
15	1.3449	0.9603	0.3905	0.2661
20	1.2969	0.9667	0.3789	0.2702
50	1.1395	0.9868	0.3428	0.2811
70	1.0929	0.9908	0.3314	0.2848
100	1.0597	0.9956	0.3209	0.2871

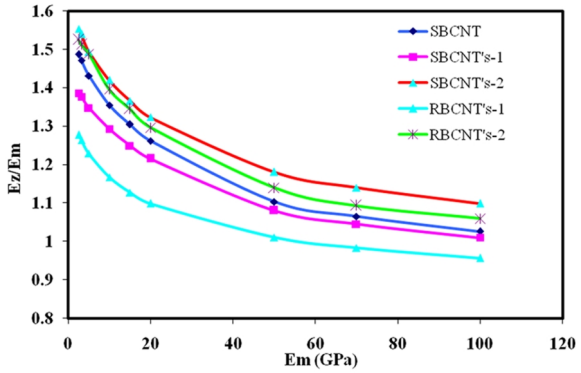

Figure 5. Variation of nanocomposite longitudinal modulus with matrix modulus

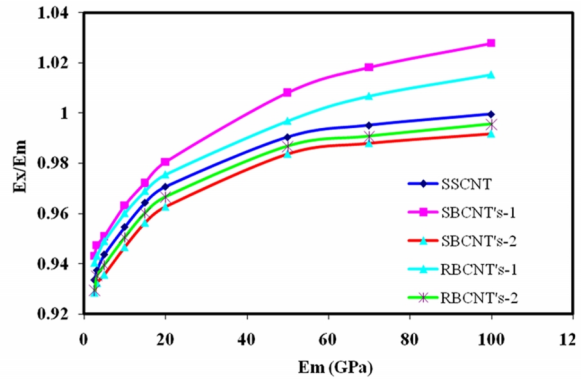

Figure 6. Variation of nanocomposite transverse modulus, $E_x=E_y$, with matrix modulus

and Poisson's ratios are also listed in this table. Comparison results obtained with results of nanocomposite reinforced with SSCNT is shown which of E_z for nanocomposite reinforced with RBCNT's is smaller E_z for nanocomposite reinforced with SSCNT. The reason is small aspect ratio of RBCNT's than SSCNT. But in transverse direction, E_x for nanocomposite reinforced with RBCNT's is larger E_x for nanocomposite reinforced with single straight CNT. The reason is small aspect ratio of RBCNT's than SSCNT and invigorate of CNT's in the transverse direction.

Then RBCNT's (model-2) is created which diameter of rope of CNT's is equal to SSCNT. Models were created to investigate the effects of matrix Young's modulus, on nanocomposite mechanical properties. The ratios of the nanocomposite longitudinal and transverse moduli to matrix modulus are listed in Table 9. These results correspond to the nanocomposite with a RBCNT's and volume fraction of 1.40%, and L/d = 12.5, $(L/d)_{RBCNT's}=5$. Nanocomposite transverse modulus and Poisson's ratios are also listed in this table. Comparison results obtained with result of nanocomposite reinforced with SSCNT is shown which of E_z for nanocomposite reinforced with RBCNT's is larger E_z for nanocomposite reinforced with SSCNT. The reason is large aspect ratio of CNT's of rope-shaped bundle than SSCNT. But in transverse direction, E_x for nanocomposite reinforced with RBCNT's is smaller E_x for nanocomposite reinforced with SSCNT. The reason is large aspect ratio of CNT's of rope-shaped bundle than SSCNT and SSCNT with same diameter with RBCNT's has greater Solidarity in the transverse direction than bundle of CNT's.

Finally, all the results are compared. This subject is shown in the Figs. 5 and 6. The results show that nanocomposites reinforced with SBCNT's greater strength than nanocomposites reinforced with RBCNT's in the longitudinal direction.

Stress contour plots of the Von Mises stresses in the SBCNT's and RBCNT's are shown in Fig. 7 (a) and (b) for the axial stretch case.

Conclusions

FEM models provide a valuable tool for the determination of mechanical properties of nanocomposite materials. In this study, FEM models

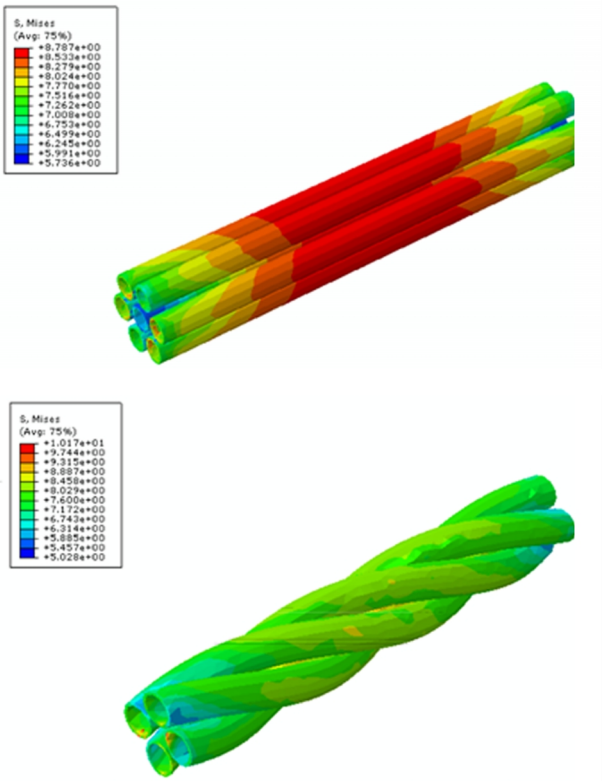

Figure 7. Plot the Von Mises stresses for (a) SBCNT's under the axial stretch ΔL, and (b) RBCNT's under the axial stretch ΔL, (E_m=100)

were developed to investigate the effects of matrix modulus on mechanical properties of nanocomposites. Studies of these effects on the mechanical properties are of highly theoretical and technological significant for nano-size fiber reinforced composites. In this study, influences of the straight bundle and rope-shaped bundle diameter, Young's modulus of matrix on the effective elastic modulus of the nanocomposites are investigated. The proposed method is very simple and easy to use. It is shown that the increases of Young's modulus of matrix and straight bundle and rope-shaped bundle diameter can significantly reduce the stiffening effect of the nanotubes in longitudinal fiber and increase the stiffening effect of the nanotubes in transverse fiber. In particular, the effective elastic constants of the nanocomposites in the longitudinal fiber are very sensitive to the straight bundle and rope-shaped bundle diameter. Thus, more detailed studies are needed in understanding and predicting the mechanical properties of carbon nanotube reinforced nanocomposites.

References

1. Iijima S. Helical Microtubles of Graphitic Carbon. *Nature* (London), **354**: 56-58 (1991).
2. Qian D., Wagner G. J., Liu W. K., Yu M. F., Ruoff R. S. Mechanics of Carbon Nanotubes. *Appl. Mech. Rev*. **55**: 495–533 (2002).
3. Saito R., Dresselhaus G., Dresselhaus M. S. Physical Properties of Carbon Nanotubes. London, Imperial College Press. (1998).
4. Treacy M. M. J., Ebbesen T. W., Gibson J. M. Exceptionally High Young's Modulus Observed for Individual Carbon Nanotubes. *Nature (London)*, **381**: 678–680 (1996).
5. Yakobson B. I., Brabec C. J., Bernholc J. Nanomechanics of Carbon Tubes: Instability Beyond Linear Response. *Phys. Rev. Lett.* **76** (14): 2511–2514 (1996).
6. Yu M. F., Files B. S., Arepalli S., Ruoff R. S. Tensile Loading of Ropes of Single Wall Carbon Nanotubes and Their Mechanical Properties. *Phys. Rev. Lett.* **84**: 5552–5555 (2000).
7. Yu M. F., Lourie O., Dyer M. J., Moloni K., Ruoff R. S. Strength and Breaking Mechanism of Multiwalled Carbon Nanotubes under Tensile Load. *Science*, **287**: 637–640 (2000).
8. Dalton A.B., Collins S., Muñoz E., Razal J.M., Ebron V.H., Ferraris J.P., Coleman J.N., Kim B.G., Baughman R.H. Super Tough Carbon Nanotube Composite Fibers for Electronic Textiles. *Nature,* **423**: 703-705 (2003).
9. De Pablo P.J., Graugnard E., Walsh B., Andres R.P., Datta S., Reifenberger R. A simple, reliable technique for making electrical contact to multi walled carbon nanotubes. *Appl. Phys. Lett.* **74**: 323-325 (1999).
10. Wei Y.Y., Eres G. Directed assembly of carbon nanotube electronic circuits. *Appl. Phys. Lett.* 76: 3759-3762 (2000).
11. Schadler L.S., Giannaris S.C., Ajayan P.M. Load transfer in carbon nanotube epoxy composites. *Appl. Phys. Lett.* 73: 3842-3845 (1998).
12. Vigolo B., Penicaud A., Coulon C., Sauder C., Pailler R., Journet C. Macroscopic fibers and ribbons of oriented carbon nanotubes. *Science*, **290**: 1331-1334 (2000).
13. Golestanian H., Shojaie M. Numerical characterization of CNT-based polymer composites considering interface effects. *Comput. Mater. Sci*. **50**: 731–736 (2010).
14. Li C.Y., Chou T.W. A structural mechanics approach for the analysis of carbon nanotubes. *Int. J. Solids Struct*. **40**: 2487–2499 (2003).
15. Chang T., Gao H. Size-dependent elastic properties of a single-walled carbon nanotube via a molecular mechanics model. *J. Mech. Phys. Solids* **51**: 1059–1074 (2003).
16. Wagner H.D., Vaia R.A. Nanocomposites: issues at the interface. *Mater. Today*, **7**: 38–42 (2004).
17. Sinnott S.B. Chemical functionalization of carbon nanotubes. *J. Nanosci. Nanotechnol*. **2**: 113–123 (2002).
18. Odegard G.M., Gates T.S., Wise K.E., Park C., Siochi E.J. Constitutive modeling of nanotube-reinforced polymer composites. *Compos. Sci. Technol*. **63**: 1671–1687 (2003).
19. Frankland S.J.V., Harik V.M., Odegard G.M., Brenner D.W., Gates T.S. The stress–strain behavior of polymer–nanotube composites from molecular dynamics simulation. *Compos. Sci. Technol.* **63**: 1655–1661 (2003).
20. Poulin P., Vigolo B., Launois P. Films and fibers of oriented single wall nanotubes. *Carbon*, **40**: 1741–1749 (2002).
21. Ashrafi B., Hubert P. Modeling the elastic properties of carbon nanotube array/polymer composites. *Compos. Sci. Technol*. **66**: 387–396 (2006).
22. Zhu H.W., Xu C.L., Wu D.H., Wei B.Q., Vajtai R., Ajayan P.M. Direct synthesis of long single-walled carbon nanotube strands. *Science,* **296**: 884–886 (2002).
23. Li Y.L., Kinloch I.A., Windle A.H. Direct spinning of carbon nanotube fibers from chemical vapor deposition synthesis. *Science*, **304**: 276-278 (2004).
24. Liewa K.M., Wong C.H., Tan M.J. Buckling properties of carbon nanotube bundles. *Appl. Phys. Lett*. 87: 1901-1904 (2005).
25. Yang Q.H., Bai S., Fournier T., Li F., Wang G., Cheng H.M., Bai J.B. Direct growth of macroscopic fibers composed of large diameter SWNTs by CVD. *Chem. Phys. Lett*. **370**: 274-279 (2003).
26. Terranova M.L., Orlanducci S., Fazi E., Sessa V., Piccirillo S., Rossi M., Manno D., Serra A. Organization of single-walled nanotubes into macro-sized rectangularly shaped ribbons. Chem. *Phys. Lett*. **381**: 86-93 (2003).
27. Zhu C., Xie Z., Guo K., Formation of close-packed multi-wall carbon nanotube bundles. *Diamond Relat. Mater*. **13**: 180-183 (2004).
28. Klaus S. Scanning Tunneling Microscopy of Carbon Nanotubes and Nanocones. *Carbon,* **33**: 915-920 (1995).
29. Ning Y., Zhang X., Wang Y., Sun Y., Shen L., Yang X., Tendeloo G.V. Bulk production of multi-wall carbon nanotube bundles on sol-gel prepared catalyst. *Chem.*

Phys. Lett. **366**: 555-558 (2002).
30. Zhang X., Cao A., Wei B., Li Y., Wei J., Xu C., Wu D. Direct growth of arrays of self-organized carbon nanotube ropes. *Chem. Phys. Lett*. **351**: 183-188 (2002).
31. Shojaie M., Golestanian H. Effects of interface characteristics on mechanical properties of carbon nanotube reinforced polymer composites. *Mater. Sci. Technol.* **27** (5): 916-922 (2011).
32. Gahruei M. H., Golestanian H. Evaluation of effective mechanical properties of nanocomposites reinforced with multi-walled carbon nanotube. *Mater. Sci. Technol*., **29** (12): 1484-1491 (2013).
33. Liu J.Z., Zheng Q. S., Wang L. F., Jiang Q. Mechanical properties of single-walled carbon nanotube bundles as bulk materials. *J. Mech. Phys. solids* **53**: 123–142 (2005).
34. Golestanian H., Gahruei M. H. Effective mechanical properties of nanocomposites reinforced with wavy carbon nanotubes. *Mater. Sci. Technol*. **29** (8): 913-920 (2013).
35. Nardelli M. B., Fattebert J. L., Orlikowski D., Roland C., Zhao Q., Bernholc J. Mechanical properties, defects and electronic behavior of carbon nanotubes. *Carbon*, **38**: 1703–1711 (2000).
36. Wong E.W., Sheehan P.E., Lieber C.M. Nanobeam mechanics: Elasticity, strength, and toughness of nanorods and nanotubes. *Science*, **277**: 1971–1975 (1997).

Gómez-del Río T., Poza P., Rodríguez J., García-Gutiérrez M.C., Hernández J.J., Ezquerra T.A. Influence of single-walled carbon nanotubes on the effective elastic constants of poly(ethylene terephthalate). *Compos. Sci. Technol*. **70**: 284–290 (2010).